Energy domain versus time domain precursor fluctuations above the Verwey transition in magnetite

S. Borroni,[1] G. S. Tucker,[2,3] U. Stuhr,[3] J. Lorenzana,[4] H. M. Rønnow,[2] and F. Carbone[1,*]

[1]*Laboratory for Ultrafast Microscopy and Electron Scattering and the Lausanne Centre for Ultrafast Science, École Polytechnique Fédérale de Lausanne, CH-1015 Lausanne, Switzerland*

[2]*Laboratory for Quantum Magnetism, École Polytechnique Fédérale de Lausanne, CH-1015 Lausanne, Switzerland*

[3]*Laboratory for Neutron Scattering and Imaging, Paul Scherrer Institut, CH-5232 Villigen, Switzerland*

[4]*Institute for Complex Systems-CNR and Physics Department, University of Rome "La Sapienza," I-00185 Rome, Italy*

(Received 29 June 2018; revised manuscript received 30 January 2020; accepted 31 January 2020; published 14 February 2020)

We study the dynamics and interactions of the critical fluctuations of the Verwey transition in magnetite (Fe_3O_4) in the pretransition region by means of inelastic neutron scattering experiments on a natural single crystal. We find that a Δ_5 mode interacts strongly with a central peak of order parameter fluctuations, whose width is determined by the order parameter coherence time. This is compared with pump-probe experiments, which we formerly explained in terms of fluctuation-assisted stimulated Raman scattering. Our estimates of the order parameter correlation time from experiments in the energy domain (inelastic neutron scattering experiments) and in the time domain (pump-probe experiments) coincide, thus giving further credit to our previous interpretation of pump-probe experiments and confirming that the Verwey transition is of the order-disorder type, without phonon softening.

DOI: 10.1103/PhysRevB.101.054303

I. INTRODUCTION

Magnetite (Fe_3O_4) is the best-known magnetic material, responsible for the most common manifestations of natural magnetism, which have fascinated mankind since ancient times. From a fundamental point of view, the reason for the continuous interest in magnetite is the occurrence of a first-order transition, the so-called Verwey transition, comprised of both atomic displacements and modifications in the electronic structure. Below the transition temperature, also referred to as the Verwey temperature T_V, the symmetry of the crystal structure is lowered from cubic to monoclinic, and long-range charge and orbital order set in, with the consequent change in the ground state from conducting to insulating [1].

In the cubic phase, multiple precursor effects anticipate the Verwey transition in electronic, structural, and magnetic degrees of freedom. Continuous modifications in the optical constants, composed of redistributions of spectral weight among different energy ranges, preempt the discontinuous changes at the Verwey temperature [2,3]. The temperature dependence of different macroscopic properties is anomalous in the pretransition region. For instance, the first magnetocrystalline anisotropy constant [4,5], the magnetostriction constant [6], and the shear modulus [7,8] show a critical behavior in broad temperature ranges above the Verwey temperature. Correlations of the precursor order are the most likely origin of the above phenomena.

In previous works, we studied the pretransition region, a few tens of kelvins above T_V, by means of inelastic neutron scattering (INS) [9] and ultrafast optical spectroscopy [10]. The emerging scenario is that, above the ordering temperature, a dense liquid of polarons, the so-called trimerons [11], shows precursor order as incommensurate correlations at wave vectors determined by polaron-polaron interactions. Then, the Verwey transition proceeds via an incommensurate-to-commensurate transformation [9].

Macroscopic order across structural transitions causes the emergence of new modes in the spectral response from inelastic scattering of light, upon folding from finite wave vectors to the center of the Brillouin zone in the ordered phase. In a recent pump-probe study, some of us argued that, close enough to the transition temperature, precursor effects make the folded modes observable also above the ordering temperature by a mechanism dubbed fluctuation-assisted stimulated Raman scattering (FASRS) [10]. In particular, it was shown that finite-momentum modes (at the Δ and X points) become Raman active in the cubic phase, thanks to the involvement of order parameter (OP) fluctuations with opposite momenta.

Observations from light probes and the occurrence of central peaks and anomalously broad phonon peaks in INS raise the important question of whether these responses in the energy domain at finite wave vectors (INS experiments) and in the time domain at zero wave vector (pump-probe experiments) can be related, as expected from theory [10]. In the following, to better understand the characteristics of the critical fluctuations, we report an INS study of the diffusive modes at the Δ point, with a focus on how they couple to the phonon modes in the cubic phase. Data from light and neutron probes are combined together to compare the characteristic timescales in both types of experiments.

The reason for the choice of the Δ point in our INS study is twofold. A symmetry analysis based on group theory identified the Δ_5 mode as a primary OP for the structural transition

*Corresponding author: fabrizio.carbone@epfl.ch

[12,13]. Indeed, even according to the most recent structural refinements, the atomic displacements from the parent to the distorted phase along the eigenvectors of Δ_5 symmetry are the largest in amplitude [11,14]. Moreover, according to the interpretation of Ref. [10], data from light probes contain information from the Δ and the X points [10]. Therefore, comparison is especially suited at these wave vectors.

This paper will be structured as follows. First, we will discuss our INS data and the model that allows extracting the characteristic timescale of the structural fluctuations. Then, we will draw a comparison with the results obtained by ultrafast optical spectroscopy and present our conclusions.

II. METHODS

A natural single crystal of magnetite of 1.7 g mass was purchased from Surface Preparation Laboratory, Zaandam, Netherlands. INS measurements were performed at the thermal triple-axis neutron spectrometer EIGER, located at the Swiss Spallation Neutron Source, Paul Scherrer Institute, Switzerland [15].

Our sample is composed of a cylinder 12 mm in length, 6 mm in diameter, and with the axis parallel to the [111] direction. In our previous INS experiments, discussed in Ref. [9] and focused on both phases, the same sample was used. To prevent crystal microtwinning in the monoclinic phase, our sample was then inserted into an aluminum ring. In our new experiments, focused on the cubic phase alone, to avoid possible damage, our sample was not removed from the aluminum ring. Again, INS measurements were carried out in the [010] zone. Our sample was installed in a standard helium cryostat, which provides precise temperature control down to 1.5 K.

Details of our previous ultrafast broadband spectroscopy experiments are available in Ref. [10]. In summary, trains of 50-fs optical pump pulses at 3.1-eV photon energy and 100-fs optical probe pulses, broadband in the visible spectral range, were delivered to the sample surface, with a repetition rate of, respectively, 3 and 6 kHz. The pump pulses were responsible for the impulsive photoexcitation of the material. The probe pulses were reflected onto the sample surface, within the same spot, to measure the time dependence of the differential optical properties, upon changing the time offset between pulse trains.

In the following, the reflections will be indexed according to the cubic scheme, $\boldsymbol{Q} = \frac{2\pi}{a}(h\boldsymbol{i} + k\boldsymbol{j} + l\boldsymbol{k}) \equiv (h, k, l)$, where $a = 8.3631$ Å is the lattice parameter in the cubic phase. The critical temperature of the structural transition was determined with higher accuracy in our new experiments by measuring the elastic intensity at (3.5, 0, 4), a superlattice reflection of the monoclinic phase, which originates from the doubling of the unit cell in the [100] direction (see Fig. 1). Based on diffraction and resistance characterization, both the electronic and structural transitions occur at the same critical temperature, $T_V = 116$ K. The temperature range for phase coexistence extends from 114 to 118 K.

The final neutron wave vector was fixed at $k_f = 2.662$ Å^{-1}. The intensity at the detector was normalized against the flux on a low-efficiency monitor between the monochromator and the sample. Inelastic scans were performed at different temperatures, across zero energy. The presence of the (1, 1, 1) and (2, 0, 0) diffraction rings of aluminum prevented measurements of the elastic peak in the (4, 0, 0) and (0, 0, 4) Brillouin zones. Therefore, in contrast to our previous INS experiments, inelastic scans were performed at (3.5, 0, 4). Elastic scans were also performed at different temperatures in two perpendicular directions in the same Brillouin zone.

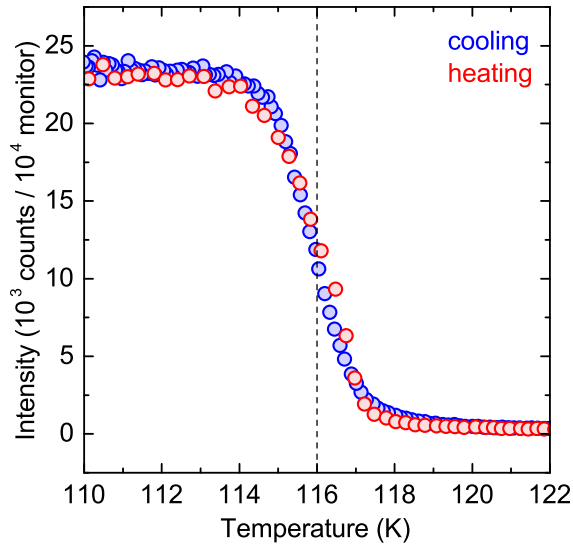

FIG. 1. Temperature dependence of the intensity of the (3.5,0,4) reflection measured on increasing and decreasing the temperature across the Verwey transition with no field applied. The heating (cooling) rates were 2.5 (−2.5) K/min for the resistance measurements and 1 (−0.5) K/min for the diffraction measurements. A vertical dashed line denotes T_V.

III. MODEL OF DIFFUSE SCATTERING IN INS

INS gives access to the mutual interactions and relative timescales of precursor order and phonons and thus enables one to gain direct insight into pretransitional phenomena. In particular, according to past INS studies of magnetite, diffuse scattering in reciprocal space is associated with intensity contributions around zero energy in the inelastic spectra, the so-called central peaks, and anomalous broadening of the phonon peaks [16].

Let us observe that, in INS, the spectral function is the Fourier transform of the time autocorrelation of the atomic displacements. Hence, clearly, the possible sources of central peaks are either propagating excitations, which have become overdamped, or diffusive excitations. The broad temperature range of the pretransitional phenomena in magnetite rules out the first possibility. In fact, even in the presence of phonon softening, typically, soft phonons are overdamped only in a narrow temperature range, around the transition temperature.

Let us then focus on the second possibility. Phenomenological models were developed to describe the spectral function in the case of continuous transitions, with diffusive excitations [17,18]. To provide a simple theoretical ground, needed for further considerations, we refer to Pak and Kinase's model [18]. The basic hypothesis is that phonon variables, i.e.,

atomic displacements $Q_{q\lambda}$, interact with pseudospin variables $\sigma_{q\lambda}$, where q and λ are, respectively, the wave vector and the branch index of the mode being considered. A pseudospin variable is a fictitious Ising operator. Depending on the system under consideration, different definitions are possible for the pseudospin lattice and the physical meaning of the pseudospin variables. In general, the two values of the pseudospin variable $\sigma_{i\lambda}$ represent local charge order in the ith cell. For instance, in Yamada's interpretation of the Verwey transition, these are the different arrangements of the extra charges among the B-type Fe ions in the primitive cell of Δ_1, Δ_4, or Δ_5 symmetry [19]. Here, we generically refer to Fourier components of pseudospin variables, $\sigma_{q\lambda} = \sum_i \sigma_{i\lambda} e^{-iq\cdot r_i}$, to represent fluctuation modes of precursor order.

Intrinsic instabilities in either or both pseudospin and phonon variables are at play in the transformation processes described by Pak and Kinase's model. In the case of magnetite, the incommensurate character and the intensity divergence of diffuse scattering at a virtual temperature below T_V, instead of at T_V, point out that the precursor effects are of second order. Therefore, they are not the direct cause of the discontinuous modifications in the crystal structure at T_V but are suitable for the application of Pak and Kinase's model.

In the following, we provide the main results of Pak and Kinase's model. The derivation of the spectral function *above the ordering temperature* starts from the equations of motion of two coupled phonon and pseudospin variables at the dominant wave vector of the instability,

$$\begin{aligned} \ddot{Q} + \gamma_Q \dot{Q} + \omega_0^2 Q &= g\sigma + E, \\ \dot{\sigma} + \gamma_\sigma\, \sigma &= gQ. \end{aligned} \tag{1}$$

For simplicity, we dropped both the wave vector q and the branch index λ. We introduced ω_0 and γ_Q, the frequency and damping constant of the phonon mode, respectively. γ_σ is the pseudospin relaxation rate, and g is the pseudospin-phonon coupling constant. E is an external field, introduced for the computation of the dynamical susceptibility, $\chi_{QQ}(\omega) = Q(\omega)/E(\omega)$.

For $g = 0$, the second equation above describes how a wave of the dominant order decays exponentially with a time constant $1/\gamma_\sigma$. For the isolated pseudospin system, assuming a second-order transition, one can postulate that the relaxation time diverges ($\gamma_\sigma \to 0$) at the nominal transition point, according to $\gamma_\sigma = \gamma_{\sigma 0}(T - T_0)/T_0$, where $\gamma_{\sigma 0}$ is a constant and T_0 is the pseudospin ordering temperature in the absence of coupling with phonons.

Equation (1) takes into account that, for finite g, the lattice displacements act as an external field polarizing the pseudospins, whereas the pseudospins act as an external force on the lattice displacements. Both systems reinforce each other, so that the second-order transition shifts to higher temperatures. The new transition point can be computed as the temperature at which the restoring force acting on the lattice in the absence of external field ($E = 0$) and for a static solution ($\ddot{Q} = \dot{Q} = \dot{\sigma} = 0$) is zero,

$$T_c = T_0\left(1 + \frac{g^2}{\gamma_{\sigma 0}\omega_0^2}\right). \tag{2}$$

In the critical region, for $T > T_V$, the system behaves as if there were a second-order transition at T_c, which, however, is cut off by the weakly first-order transition at $T_V > T_c$.

We define a phonon spectral function from the imaginary part of the dynamic susceptibility, according to the fluctuation-dissipation theorem,

$$\begin{aligned} \phi_{QQ}(\omega) &= 2[1 + n(\omega)]\ \mathrm{Im}[\chi_{QQ}(\omega)] \\ &= 2[1 + n(\omega)]\ \frac{\omega g^2/\gamma_\sigma^2}{\left(\widetilde{\omega}_0^2 - \omega^2\right)^2 + \omega^2\widetilde{\gamma}^2}. \end{aligned} \tag{3}$$

Here, $1 + n(\omega) = [1 - \exp(-\omega/k_B T)]^{-1}$ is the Bose-Einstein thermal factor. $\widetilde{\omega}_0^2$ and $\widetilde{\gamma}$ are, respectively, a squared renormalized frequency and a frequency-dependent damping coefficient, defined by

$$\widetilde{\omega}_0^2 = \frac{\omega_0^2\gamma_\sigma - g^2}{\gamma_\sigma + \gamma_Q}, \tag{4}$$

$$\widetilde{\gamma} = \frac{\omega_0^2 + \gamma_\sigma\gamma_Q - \omega^2}{\gamma_\sigma + \gamma_Q}. \tag{5}$$

Shapiro *et al.* fit the spectral response at (4, −0.2, −0.2) and (4, 0, 3.25) at 125 and 150 K with Yamada's model function, which is equivalent to Eq. (3), but with $\gamma_Q = 0$, i.e., negligible phonon damping [16,17]. Their results, combined with our failure to observe any phonon softening [9], suggest that intrinsic instabilities of the pseudospin variables, with slow dynamics compared to the phonon variables, represent the initial driving forces for the transition process.

IV. COMPARISON BETWEEN INS AND ULTRAFAST OPTICAL SPECTROSCOPY

Figures 2(a) and 2(b) show the distribution of the elastic scattering intensity in reciprocal space around the (4, 0, 4) reflection, along the [Q_h 0 4] and [3.66 0 Q_l] directions, as a function of temperature. The unchanged features around (3.66, 0, 4.3) and (2.7, 0, 4) are artifacts, which probably originate, respectively, from the (2, 2, 0) diffraction ring of aluminum and a ⟨2, 2, 4⟩ reflection of a misaligned crystallite. In the absence of diffuse scattering, in the cubic phase, far enough from the transition temperature, and in the monoclinic phase, the base intensity originates from incoherent scattering alone. Indeed, intensity levels are comparable around (3.2, 0, 4) at 105 K $< T_V$ and 180 K $\gg T_V$ and thus are here regarded as our reference for incoherent scattering. Below T_V, superlattice reflections appear at the half-integer indexes (2.5, 0, 4) and (3.5, 0, 4), upon unit cell doubling, and at the even-odd mixed index (3, 0, 4), for the breaking of the translational symmetry along the ⟨100⟩ directions [16]. Diffuse scattering is responsible for the progressive buildup of intensity above the background observable in the 125–180 K temperature range. The narrow feature around (3.66, 0, 4) in Fig. 2(b) points out the streaklike character of diffuse scattering in the [100] direction at all temperatures. The pronounced intensity of the $E = 0$ constant-Q scans in the Q_h = 3.1–3.3 range at 138 and 125 K in Fig. 2(a) signals the incommensurate nature of diffuse scattering in the same temperature range. The bumps observable around (3, 0, 4) and (3.5, 0, 4) at the temperature closest to T_V, 120 K = T_V +

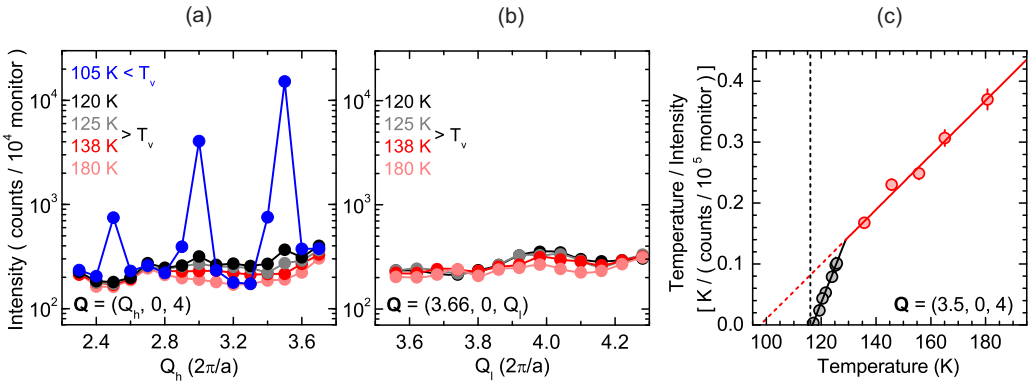

FIG. 2. Wave-vector and temperature dependence of elastic scattering intensity across the Verwey transition. Elastic scattering intensity as a function of wave vector along the lines (a) from $Q_h = 2.3$ to $Q_h = 3.7$ and (b) from $Q_l = 3.56$ to $Q_l = 4.28$ in the orthogonal directions $Q_l = 4$ and $Q_h = 3.66$ (red and black shades) at different temperatures above T_V and (blue) at 105 K $< T_V$. Error bars lie within data points. Lines are guides to the eye. (c) Temperature dependence of the inverse intensity of diffuse scattering corrected for the thermal factor. Solid lines are linear fits to the data in different critical regimes between T_V and 129 K (black) and above 129 K (red). A red dashed line indicates the virtual instability of the critical regime above 129 K. A vertical dashed line denotes T_V.

4 K, are related to the appearance of new Bragg peaks at the same wave vectors in the monoclinic phase and are generally referred to as spotlike scattering to distinguish them from diffuse scattering.

Figure 2(c) shows the temperature dependence of the inverse intensity of critical scattering, multiplied by the temperature, to account for the occupation number of the diffusive excitations at the origin of critical scattering. Our reference for incoherent scattering is subtracted from the scattering intensity to single out the contribution from critical scattering alone. A piecewise fit with linear functions identifies two critical regimes, above 129 K and between T_V and 129 K, which are denoted with red and black shades, respectively, in the color coding of Figs. 2(c) and 3. The extrapolation of the temperature-to-intensity ratio to zero for the critical regime above 129 K provides the approximate estimate $T_c = 97.7 \pm 14.7$ K. Instead, in the critical regime between T_V and 129 K, clearly, the scattering intensity diverges at T_V.

Figure 3(a) shows the temperature dependence of the central peak at the Δ point and the transverse acoustic (TA) Δ_5 mode in the cubic phase. The elastic peak at (3.5, 0, 4) and 180 K, far enough from the transition temperature, is here assumed as our reference for the incoherent peak and subtracted from all the inelastic spectra at lower temperature and the same point in reciprocal space. The model function defined by Eqs. (3), (4), and (5) is convolved with the resolution function of the spectrometer and fit to the data. To provide reasonable constraints, a simultaneous fit analysis, with common values of the fitting parameters T_0 and T_c, is carried out for the data set in the critical regime above 129 K. The following expressions provide approximate estimates of the linewidths of the central peak, Γ_{cp}, and the phonon peak, Γ_{ps}, corrected for the experimental resolution:

$$\Gamma_{cp} = \frac{2\omega_0^2\gamma_{\sigma 0}(T - T_c)/T_0}{\omega_0^2 + \gamma_Q\gamma_{\sigma 0}(T - T_0)/T_0}. \quad (6)$$

$$\Gamma_{ps} = \frac{\gamma_{\sigma 0}}{\omega_0 T_0}\sqrt{2(T - T_0)^2\gamma_Q^2 + (T_c - T_0)^2\omega_0^2}. \quad (7)$$

In turn, under the assumption of a single decay channel, the correlation time of the excitation responsible for the central peak is evaluated according to $\tau = 2\hbar/\Gamma_{cp}$. The model

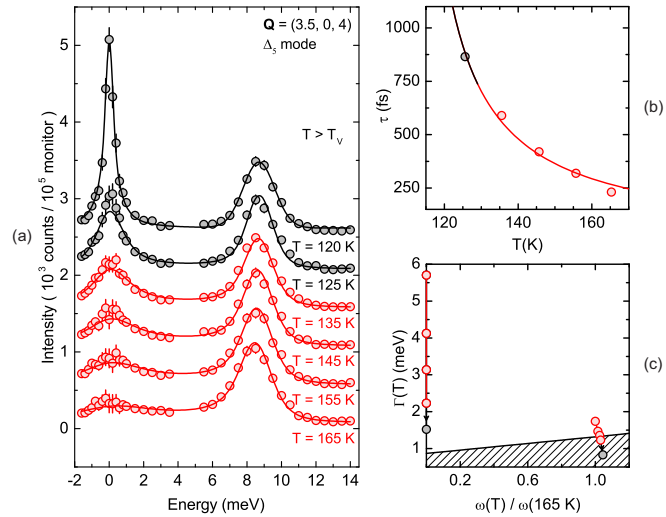

FIG. 3. (a) Inelastic spectra at the Δ point (3.5, 0, 4) at different temperatures above T_V in the energy range from -1.6 to 14 meV, which contains the elastic peak and the Δ_5 mode. For clarity, error bars are doubled, and data points at different temperatures are offset by 5×10^2 counts/10^5 monitor. The estimate of the incoherent peak from the data at 180 K and at the same point in reciprocal space is subtracted from all the inelastic spectra. Lines in the 125–165 K temperature range are fits to the data according to the model function defined by Eqs. (3), (4), and (5). The line at 120 K is a guide to the eye. (b) Estimate of the inverse linewidth of the central peak as a function of temperature from the fit analysis. The line is a guide to the eye. (c) Temperature dependence of the two poles of the dynamical susceptibility in the first quadrant of the complex plane. The real and imaginary parts of the poles correspond, respectively, to the energy and linewidth of the central peak and the phonon peak. Red (black) denotes the critical regime above 129 K (between T_V and 129 K). The hatched area represents the instrumental resolution, within which estimates are not reliable.

TABLE I. Parameter values from fit analysis.

T (K)	γ_σ	γ_Q (meV)	T_0 (K)	T_c (K)	Γ_{cp} (meV)	Γ_{ps} (meV)	τ (fs)
165	0.48	0.29	56	94	5.7	1.7	230
155	0.41	0.23	56	94	4.1	1.5	320
145	0.37	0.11	56	94	3.1	1.4	420
135	0.34	0.00	56	94	2.2	1.2	590
125	0.28	0.00	60	95	1.5	0.8	870

function does not apply to the data at 120 K, owing to the onset of spotlike scattering. However, the instrumental resolution provides a lower boundary for τ at 120 K. The fitting functions are superimposed on the data in Fig. 3(a). The fit results and the approximate estimates of Γ_{cp} Γ_{ps} and τ are summarized in Table I. τ is plotted against temperature in Fig. 3(b). Figure 3(c) shows the energy and linewidth of the central peak and the phonon peak at different temperatures, in analogy to Fig. 1(a) of Ref. [18], to emphasize the agreement with the case of pseudospin ordering, with slow pseudospin relaxation and meaningful pseudospin-phonon coupling. Pak and Kinase computed the above quantities as the real and imaginary parts of the poles of the dynamical susceptibility, respectively.

To compare data from neutron and light probes, let us summarize the results discussed in Ref. [10]. Two oscillations of the optical functions were observed upon impulsive photoexcitation and assigned to the monoclinic counterparts of the X_3 mode and the transverse optical (TO) mode of Δ_2 symmetry, hereafter simply labeled as the Δ_2 mode. The coherent response, averaged in two different temperature ranges to improve the signal-to-noise ratio, is shown in Fig. 4(a). The fit components corresponding to each oscillation are also plotted. Figure 4(b) displays the power spectrum of the oscillations. All the modes under discussion are shown in Fig. 4(c). In the 10–75 K temperature range, the modes are at the center of the Brillouin zone, and the photoexcitation mechanism is transient stimulated Raman scattering (TSRS) of the first order [see Fig. 4(a), lower time trace] [20,21]. Instead, in the 130–140 K temperature range, the modes are at finite wave vectors but are still observable through FASRS [see Fig. 4(a), upper time trace]. Vertical arrows in Fig. 4(a) indicate approximate estimates of the coherence time of the oscillation of the Δ_2 mode, $\tau_m = 460$ fs and $\tau_c = 240$ fs, respectively, in the monoclinic and cubic phases.

V. DISCUSSION AND CONCLUSIONS

To provide a basis to describe the critical dynamics of the Verwey transition and thus interpret our complete set of observations, let us consider the expansion of the free-energy density to the fourth order over the power series of phonon and pseudospin variables of any possible wave vector $\boldsymbol{q}$ and branch index λ,

$$\begin{aligned}\mathcal{F}(\{Q_{q\lambda},\sigma_{q\lambda}\}) = &\sum_{q\lambda}\omega_{q\lambda}^2 Q_{q\lambda}^* Q_{-q\lambda} + \sum_{q\lambda}\chi_{\sigma q\lambda}^{-1}\sigma_{q\lambda}^*\sigma_{-q\lambda}\\ &+\sum_{q\lambda} g_{q\lambda}(Q_{q\lambda}^*\sigma_{-q\lambda} + Q_{-q\lambda}\sigma_{q\lambda}^*)\\ &+\sum_{\substack{q_1q_2\\ q_3\lambda}} g'_{\substack{q_1q_2\\ q_3\lambda}}\left(\sigma_{q_1\lambda}\sigma_{q_2\lambda} + \sigma_{q_1\lambda}^*\sigma_{q_2\lambda}^*\right)\\ &\times Q_{q_3\lambda}\delta_{q_1+q_2+q_3+G} + \cdots, \end{aligned} \tag{8}$$

where $\cdots$ indicate positive terms of the fourth order. The translational symmetry of the Hamiltonian reflects into the free-energy density and requires that $\boldsymbol{q}_1 + \boldsymbol{q}_2 + \boldsymbol{q}_3$ is equal to a reciprocal lattice vector $\boldsymbol{G}$.

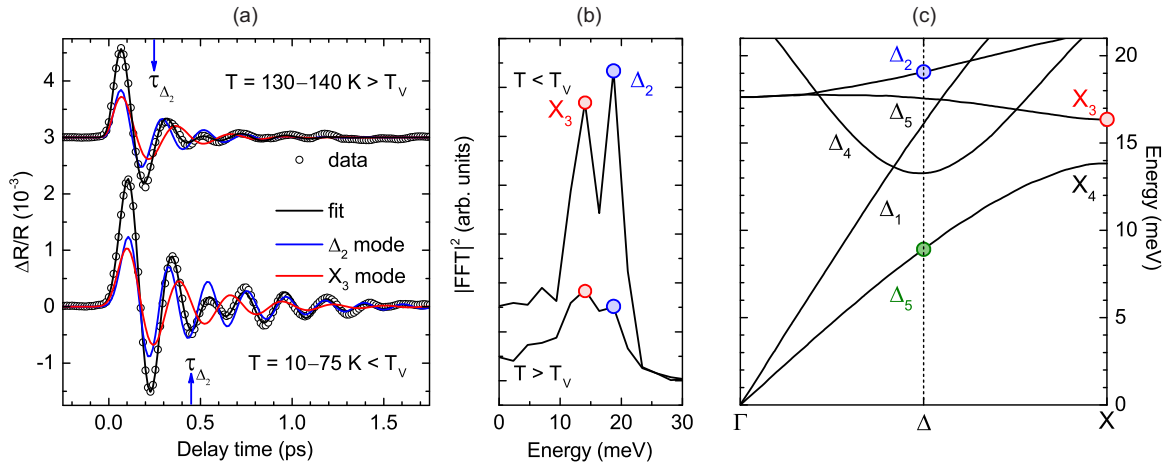

FIG. 4. (a) Coherent oscillations of the differential reflectivity as a function of pump-probe delay time, averaged between 2.0− and 2.3-eV probe photon energy, and in two different temperature ranges, below (10–75 K, lower time trace) and above T_V (130–140 K, upper time trace). Data (fitting functions) are plotted with symbols (lines). Blue (red) corresponds to the Δ_2 (X_3) mode. Black is associated with the total fit functions. Vertical arrows indicate approximate estimates of the coherence time of the Δ_2 mode. (b) Power spectrum of the coherent oscillations from a Fourier transform of the data in (a). (c) *Ab initio* calculations of the phonon dispersion curves in the cubic phase along the ⟨100⟩ directions (lines). A vertical dashed line denotes the Δ point. Symbols and colored labels indicate the modes at the focus of our experiments: the TA Δ_5 mode, studied in the energy domain in our INS experiments (green), and the TO Δ_2 (blue) and X_3 (red) modes, studied in the time domain in our pump-probe experiments.

Far enough from T_V, the amplitude of the critical fluctuations is small. In general, terms of second order in σ are negligible. However, intrinsic instabilities of the pseudospin variables cause terms with large generalized susceptibility $\chi_{\sigma \boldsymbol{q} \lambda}$, responsible for precursor effects with continuous character. The most unstable modes are located at incommensurate wave vectors around $\langle 0.75, 0, 0 \rangle$ [16,22–24]. In the following, let us consider the modes at $\langle 0.5, 0, 0 \rangle$ and the TA branch, at the focus of our experiments. For simplicity, we drop the wave vector $\boldsymbol{q}$ and branch index λ, and we treat Q and σ as real variables. Accordingly, the explicit expression of the nonnegligible terms in the small-amplitude regime is

$$\mathcal{F}(Q, \sigma) = \omega_0^2 Q^2 + \gamma_{\sigma 0} \sigma^2 (T - T_0)/T_0 + 2gQ\sigma + \beta Q^4 + \gamma \sigma^4, \tag{9}$$

where β and γ are positive constants. The phenomenological model introduced in Sec. III refers to the above equation. Due to the finite resolution of the spectrometer, in fact, the measured intensity of diffuse scattering is the integrated intensity around zero energy. Its approximate expression is given by the product between the $\omega \to 0$ limit of $\phi_{QQ}(\omega)$ [see Eqs. (3), (4), and (5)] and Γ_{cp} [see Eq. (6)] for $\gamma_Q = 0$. As a result, in the small-amplitude regime, the temperature-to-intensity ratio scales with temperature according to $T - T_c$. Indeed, it is possible to fit the data in Fig. 2(c) with a linear function in the 135–180 K temperature range, which is thus identified with the small-amplitude regime. The fitting function extrapolates to zero temperature-to-intensity ratio at $T_c < T_V$. Therefore, T_c represents the spinodal point of the first-order transition.

Fluctuations of significant amplitude develop near T_V. As a consequence, linear-quadratic Q-σ coupling is not negligible anymore. On the contrary, it grows into the dominant terms, which govern the discontinuous modifications at T_V. In particular, according to the explanation first advanced by Iizumi with reference to the structural degree of freedom [25], the third-order terms prevail over the energy gain from the onset of incommensurate fluctuations, and they eventually lock in the monoclinic phase.

In the critical regime between T_V and 129 K, the data in Fig. 2(c) lie on a straight line, which crosses zero at T_V. This resembles the characteristic divergence of the susceptibility in a continuous transition. In principle, different interpretations of the onset of spotlike scattering can be proposed. For instance, it is possible to argue that, in contrast to diffuse scattering, spotlike scattering is observable only over a narrow temperature range above T_V, which is consistent with the typical temperature dependences of overdamped excitations in phase transitions. However, some of us provided conclusive evidence that the Δ_5 mode does not soften [9]. In fact, the general interpretation of the Verwey transition proposed in Ref. [9] rules out the occurrence of phonon softening altogether. Moreover, overdamped excitations are supposed to show a noticeable change in intensity profile as a function of temperature, with progressive transfer of spectral weight from finite to zero energy. This is clearly incompatible with the characteristics of the central peak of spotlike scattering in our observations, centered at zero energy and within the instrumental resolution [see Fig. 3(a)].

It is also arguable whether critical scattering in general is essential to the mechanism of the Verwey transition or a consequence of the impurity content in natural single crystals of magnetite such as our sample. In this regard, let us note that spotlike scattering was not always observed, in contrast to diffuse scattering, which was reported also in systematic studies on synthetic samples with controlled stoichiometry [16,22–24,26–28].

Let us now discuss the comparison between data from neutron and light probes. In Ref. [10], some of us showed that in the cubic phase the time dependence of the correlation between the fluctuations of the ordering field and the atomic displacements upon impulsive photoexcitation $\langle \rho_{\boldsymbol{q}} Q_{-\boldsymbol{q}} \rangle$ modulates the optical response through its dependence on the dielectric susceptibility $\boldsymbol{\chi}$. It was also shown that, in turn, the time dependence of $\langle \rho_{\boldsymbol{q}} Q_{-\boldsymbol{q}} \rangle$ can be computed via the Kubo formula in the response regime linear in fluence under the assumption of a classical ordering field. We now introduce the additional hypothesis of a relaxational response of the critical fluctuations with a single relaxation time $\tau_{\rho \boldsymbol{q}}$, such that the autocorrelation of fluctuations of the ordering field can be expressed as

$$\langle \rho_{\boldsymbol{q}}(t) \rho_{-\boldsymbol{q}}(t') \rangle = \langle \rho_{\boldsymbol{q}} \rho_{-\boldsymbol{q}} \rangle \, e^{-(t-t')/\tau_{\rho \boldsymbol{q}}}. \tag{10}$$

Let us note that the equal-time autocorrelation $\langle \rho_{\boldsymbol{q}} \rho_{-\boldsymbol{q}} \rangle$ is a constant because correlation functions are stationary. The time dependences of the correlations that govern the coherent response in the cubic and monoclinic phase can thus be written as Eqs. (11) and (12), respectively. In the monoclinic phase, the coherent phonons generated via TSRS [21] are at $\boldsymbol{q} = 0$.

$$\langle \rho_{\boldsymbol{q}} Q_{-\boldsymbol{q}} \rangle(t) = -\int_{-\infty}^{t} dt' \langle \rho_{\boldsymbol{q}} \rho_{-\boldsymbol{q}} \rangle \frac{e^{-(t-t')/\tau_{\boldsymbol{q}}} \sin[\omega_{\boldsymbol{q}}(t-t')]}{\omega_{\boldsymbol{q}}} \times g_{\boldsymbol{q}}(t'), \quad T > T_V. \tag{11}$$

$$\langle Q_0 \rangle(t) = -\int_{-\infty}^{t} dt' \frac{e^{-(t-t')/\tau_{ph}} \sin[\omega_0(t-t')]}{\omega_0} \times g_0(t'), \quad T < T_V. \tag{12}$$

Different effective forces $g_{\boldsymbol{q}}$ and g_0 act in the excitation processes of FASRS and TSRS, respectively, in the cubic and monoclinic phases [10,21]. In the cubic phase, the coherence time of each oscillation, labeled $\tau_{\boldsymbol{q}}$, is determined by the competition of two different processes, namely, the loss of phase memory of the coherent phonon and the correlation decay of the critical fluctuations. To a first approximation, let us assume that for equal fluence the effects of oscillation dephasing are the same in the temperature range from 10 to 140 K, and thus, the faster damping in the cubic phase compared to the monoclinic phase is only due to the assistance of critical fluctuations in the excitation process. Indeed, the duration of each oscillation does not change noticeably throughout the monoclinic phase. Under the above simplifying assumption, the coherence time of each oscillation in the monoclinic phase constitutes an approximate estimate of the phenomenological phonon lifetime τ_{ph}. Therefore, the coherence times above and

below the transition temperature are related by

$$\frac{1}{\tau_{\boldsymbol{q}}} = \frac{1}{\tau_{ph}} + \frac{1}{\tau_{\rho\,\boldsymbol{q}}}. \tag{13}$$

Hereafter, let us refer to the Δ_2 mode and the ordering field mode at the Δ point, which are coupled to each other by the impulsive photoexcitation (the wave vector $\boldsymbol{q}$ is dropped). Equation (13) provides an approximate estimate of the correlation time of the ordering field, $\tau_\rho = (\tau_c^{-1} - \tau_m^{-1})^{-1} \approx 0.5$ ps.

The condensation of atomic displacements of Δ_5 symmetry in the monoclinic phase provides the most important contribution to the intensity of the superlattice reflections at the Δ point, with particular reference to (3.5, 0, 4), the focus in our INS experiments [19] [the dynamical factor of the Δ_5 mode at (0.5, 0, 8) and $(4 \pm 0.5, 0, 8)$ is even larger; however, neither of them was accessible]. Therefore, the symmetry of the fluctuation mode that gives rise to the central peak at the Δ point must be Δ_5. Our observation of strong coupling between the central peak at the Δ point itself and the TA Δ_5 mode is further confirmation. Indeed, in order for the Hamiltonian to be totally symmetric, in each term of bilinear coupling, the symmetry of the fluctuation mode needs to be the same as that of the phonon mode [see Eq. (8)]. Notice that, in addition to the TA Δ_5 mode studied in our INS experiments [green in Fig. 4(c)], there is another Δ_5 mode [black in Fig. 4(c)] which is close in energy to the Δ_2 mode of our pump-probe experiments. Due to limitations of energy resolution, both modes were considered as candidates for the identification of the faster of the coherent oscillations in Ref. [10]. To provide a reliable assignment, the Raman matrix elements were computed as a function of probe photon energy. It was concluded that the assumption of Δ_2 symmetry results in the best agreement between calculations and experimental data. This implies that also the associated fluctuation mode must be of Δ_2 symmetry.

Thus, we are in the presence of two central peaks, related to fluctuation modes of Δ_5 and Δ_2 symmetries, appearing, respectively, in INS and pump-probe experiments. To gain further insight, we compare their correlation times. In the same temperature range around 135 K, the correlation times measured with neutron and light probes are both close to 0.5 ps. This suggest two possible scenarios for the symmetry of the fluctuations. It may be that fluctuations of different symmetries are soft above the Verwey temperature and no dominant symmetry emerges until trimeron order condenses. It may otherwise be that only fluctuations of Δ_5 symmetry are relevant and the assignment of Ref. [10] must be revised. Notice that such an assignment was done based on density functional theory computations of excitation spectra in a strongly correlated material, which is a notoriously difficult problem. Irrespective of symmetry considerations, it is reassuring to remark the similarity between correlation times measured with different probes. This further validates the FASRS mechanism that we proposed in Ref. [10].

In summary, INS experiments confirm our previous interpretation, based on pump-probe experiments, that long-lived fluctuations (0.5 ps) of trimeron order appear above the ordering temperature. The spectrum of such fluctuations is centered at zero energy but carries momentum, so that it can assist with the appearance of finite-momentum modes in the Raman response without significantly modifying their energy. In addition, such results confirm the picture of the Verwey transition as an order-disorder transition without phonon softening. The symmetry of the fluctuations remains an open problem since INS and pump-probe experiments provide different results.

ACKNOWLEDGMENTS

We acknowledge A. M. Oleś (Marian Smoluchowski Institute of Physics, Jagiellonian University, Kraków) and P. Piekarz (Institute of Nuclear Physics, Polish Academy of Sciences, Kraków) for useful discussions and D. Rubin (Soreq Nuclear Research Center, Yavne) for the design of the sample holder. LUMES acknowledges financial support from the NCCR MUST. H.M.R. acknowledges financial support from the Swiss National Science Foundation and its Sinergia network Mott Physics Beyond the Heisenberg model (MPBH). J.L. acknowledges financial support from Italian MIUR through Project No. PRIN 2017Z8TS5B, and from Regione Lazio (L. R. 13/08) under project SIMAP.

[1] F. Walz, The Verwey transition – A topical review, J. Phys.: Condens. Matter **14**, R285 (2002).

[2] S. K. Park, T. Ishikawa, and Y. Tokura, Charge-gap formation upon the Verwey transition in Fe_3O_4, Phys. Rev. B **58**, 3717 (1998).

[3] F. Randi, I. Vergara, F. Novelli, M. Esposito, M. Dell'Angela, V. A. M. Brabers, P. Metcalf, R. Kukreja, H. A. Dürr, D. Fausti *et al.*, Phase separation in the nonequilibrium Verwey transition in magnetite, Phys. Rev. B **93**, 054305 (2016).

[4] R. Aragón, Cubic magnetic anisotropy of nonstoichiometric magnetite, Phys. Rev. B **46**, 5334 (1992).

[5] R. Řezníček, V. Chlan, H. Štěpánková, P. Novák, and M. Maryško, Magnetocrystalline anisotropy of magnetite, J. Phys.: Condens. Matter **24**, 055501 (2012).

[6] V. Brabers and J. Hendrinks, Magnetostriction of aluminium substituted magnetite, J. Magn. Magn. Mater. **26**, 300 (1982).

[7] H. Schwenk, S. Bareiter, C. Hinkel, B. Lüthi, Z. Kakol, A. Koslowski, and J. Honig, Charge ordering and elastic constants in $Fe_{3-x}Zn_xO_4$, Eur. Phys. J. B **13**, 491 (2000).

[8] M. M. Seikh, C. Narayana, P. A. Metcalf, J. M Honig, and A. K. Sood, Brillouin scattering studies in Fe_3O_4 across the Verwey transition, Phys. Rev. B **71**, 174106 (2005).

[9] S. Borroni, G. S. Tucker, F. Pennacchio, J. Rajeswari, U. Stuhr, A. Pisoni, J. Lorenzana, H. M. Ronnow, and F. Carbone, Mapping the lattice dynamical anomaly of the order parameters across the Verwey transition in magnetite, New J. Phys. **19**, 103013 (2017).

[10] S. Borroni, E. Baldini, V. M. Katukuri, A. Mann, K. Parlinski, D. Legut, C. Arrell, F. van Mourik, J. Teyssier, A. Kozlowski

et al., Coherent generation of symmetry-forbidden phonons by light-induced electron-phonon interactions in magnetite, Phys. Rev. B **96**, 104308 (2017).

[11] M. S. Senn, J. P. Wright, and J. P. Attfield, Charge order and three-site distortions in the Verwey structure of magnetite, Nature (London) **481**, 173 (2012).

[12] P. Piekarz, K. Parlinski, and A. M. Oleś, Mechanism of the Verwey Transition in Magnetite, Phys. Rev. Lett. **97**, 156402 (2006).

[13] P. Piekarz, K. Parlinski, and A. M. Oleś, Origin of the Verwey transition in magnetite: Group theory, electronic structure, and lattice dynamics study, Phys. Rev. B **76**, 165124 (2007).

[14] M. S. Senn, J. P. Wright, J. Cumby, and J. P. Attfield, Charge localization in the Verwey structure of magnetite, Phys. Rev. B **92**, 024104 (2015).

[15] U. Stuhr, B. Roessli, S. Gvasaliya, H. M. Rønnow, U. Filges, D. Graf, A. Bollhalder, D. Hohl, R. Bürge, M. Schild *et al.*, The thermal triple-axis-spectrometer EIGER at the continuous spallation source SINQ, Nucl. Instrum. Methods Phys. Res., Sect. A **853**, 16 (2017).

[16] S. Shapiro, M. Iizumi, and G. Shirane, Neutron scattering study of the diffuse critical scattering associated with the Verwey transition in magnetite (Fe_3O_4), Phys. Rev. B **14**, 200 (1976).

[17] Y. Yamada, H. Takatera, and D. L. Huber, Critical dynamical phenomena in pseudospin-phonon coupled systems, J. Phys. Soc. Jpn. **36**, 641 (1974).

[18] K. N. Pak and W. Kinase, Dynamic critical behaviors of pseudospin-phonon coupled system, J. Phys. Soc. Jpn. **38**, 1 (1975).

[19] Y. Yamada, C. Graham, Jr., G. Lander, and J. Rhyne, Charge ordering and lattice instability in magnetite, in *Magnetism and Magnetic Materials-1974: 20th Annual Conference, San Francisco*, edited by C. D. Graham, Jr., G. H. Lander, and J. J. Rhyne, AIP Conf. Proc. No. 24 (AIP, New York, 1975), p. 79.

[20] R. Merlin, Generating coherent THz phonons with light pulses, Solid State Commun. **102**, 207 (1997).

[21] T. E. Stevens, J. Kuhl, and R. Merlin, Coherent phonon generation and the two stimulated Raman tensors, Phys. Rev. B **65**, 144304 (2002).

[22] K. Chiba, K. Suzuki, and S. Chikazumi, Diffuse electron scattering from magnetite above the Verwey transition temperature, J. Phys. Soc. Jpn. **39**, 839 (1975).

[23] Y. Yamada, N. Wakabayashi, and R. M. Nicklow, Neutron diffuse scattering in magnetite due to molecular polarons, Phys. Rev. B **21**, 4642 (1980).

[24] K. Siratori, Y. Ishii, Y. Morii, S. Funahashi, S. Todo, and A. Yanase, Neutron diffuse scattering study of the high temperature phase of Fe_3O_4 − I, Determination of atomic displacements at the X point in the Brillouin zone, J. Phys. Soc. Jpn. **67**, 2818 (1998).

[25] M. Iizumi, Verwey transition in magnetite as a potentially incommensurate but evantually commensurate phase transition, in *Modulated Structures-1979*, edited by J. M. Cowley, J. B. Cohen, M. B. Salamon, and B. J. Wuensch, AIP Conf. Proc. No. 53 (AIP, New York, 1979), p. 184.

[26] Y. Fujii, G. Shirane, and Y. Yamada, Study of the 123-K phase transition of magnetite by critical neutron scattering, Phys. Rev. B **11**, 2036 (1975).

[27] R. Aragón, P. M. Gehring, and S. M. Shapiro, Stoichiometry, Percolation, and Verwey Ordering in Magnetite, Phys. Rev. Lett. **70**, 1635 (1993).

[28] A. Bosak, D. Chernyshov, M. Hoesch, P. Piekarz, M. Le Tacon, M. Krisch, A. Kozłowski, A. M. Oleś, and K. Parlinski, Short-Range Correlations in Magnetite Above the Verwey Temperature, Phys. Rev. X **4**, 011040 (2014).